Finite element modelling of elastic wave scattering in a polycrystalline material in two and three dimensions

Anton Van Pamel

Imperial College London

Department of Mechanical Engineering

Exhibition Road

London, SW7 2AZ, UK

Peter Huthwaite

Imperial College London

Department of Mechanical Engineering

Exhibition Road

London, SW7 2AZ, UK

Colin R. Brett

E.ON Technologies (Ratcliffe) Ltd. E.ON Technologies (Ratcliffe) Limited

Technology Centre, Ratcliffe-on-Soar,

Nottingham, NG11 0EE, UK

Michael J. S. Lowe[1]

Imperial College London

Department of Mechanical Engineering

Exhibition Road

London, SW7 2AZ, UK

[1] m.lowe@imperial.ac.uk

Manuscript accepted for publication in J. Acoust. Soc. Am 128 (3), September 2015.

Abstract - Finite Element modelling is a promising tool for further progressing the development of ultrasonic NDE of polycrystalline materials. Yet its widespread adoption has been held back due to a high computational cost, which has restricted current works to relatively small models and to two dimensions. However, the emergence of sufficiently powerful computing, such as highly efficient solutions on graphics processors is enabling a step improvement in possibilities. This article aims to realise those capabilities, to simulate ultrasonic scattering of longitudinal waves in an equiaxed polycrystalline material in both 2D and 3D. The modelling relies on an established Voronoi approach to randomly generate a representative grain morphology. It is shown that both 2D and 3D numerical data show good agreement across a range of scattering regimes in comparison to well-established theoretical predictions for attenuation and phase velocity. In addition, 2D parametric studies illustrate the mesh sampling requirements for two different types of mesh, to ensure modelling accuracy and present useful guidelines for future works. Modelling limitations are also shown. It is found that 2D models reduce the scattering mechanism in the Rayleigh regime.

Pacs: 43.35Cg

I. INTRODUCTION

Scattering of ultrasonic waves in polycrystalline materials has been studied since the beginning of ultrasonic NDE. In a pioneering experiment, Mason and McSkimin[1] discovered a fourth order frequency dependence for the scattering induced attenuation in polycrystalline aluminium, therefore termed Rayleigh scattering in the long-wavelength regime. At higher frequencies, when the wavelength becomes dimensionally comparable to the grain size, the attenuation behaviour is dominated by a stochastic mechanism[2] where it reduces to a second order frequency dependence. Eventually, when the grain sizes are large, relative to the wavelength, there is a geometric regime[3] where attenuation becomes frequency independent. Mathematical solutions to predict attenuation soon followed: foundations were laid by Lifshits and Parkhamvoski[4], Bhatia and Moore[5], Rohklin[6], Hirsekorn[7], and Kino and Stanke[8]. The approach by Kino and Stanke obtains attenuation for an idealised cubic polycrystalline material, valid across all regimes of scattering, and stands today as the Unified Theory.

Models such as the Unified Theory have proven particularly useful to characterise polycrystalline materials by inversion from attenuation measurements[9,10]. For ultrasonic flaw detection however, the scattering induced grain noise is also of interest. In attempts to improve ultrasonic inspections[11], which are limited by the signal to coherent noise ratio, efforts turned towards predicting the backscatter from microstructural noise[12]. This eventually led to the Independent Scattering Model[13] (ISM) which has significantly benefited ultrasonic inspections[14] today. However, the ISM neglects multiple scattering which thus limits its applicability to relatively weak scattering media[15].

More recently, researchers[16-20] have considered Finite Element (FE) modelling to overcome this limitation and confront more challenging scattering scenarios. In contrast to existing theoretical approaches, its ability to simulate time-domain signals, incorporating both attenuation and noise, whilst also including complex physics such as multiple scattering[17], makes FE a promising candidate. Its flexibility and high fidelity will probably be instrumental to further progressing the development of ultrasonic NDE of polycrystalline materials.

Yet its widespread adoption has been held back due to a high computational cost which arises from having to numerically discretise the material's microstructure. This has restricted current works to relatively small models e.g. of the order of 1000s of grains, which, while representing impressive progress is still only sufficient for a reduced range of feasible scattering regimes, and to 2 dimensions. The latter limitation, a 2D model, obliges several simplifications including:

(1) The representation of grain size distributions of a 3D material in a 2D model. Namely, the grain cross-sections seen on a slice of a 2D material do not correctly represent the grain sizes of a 3D material.

(2) The stiffness matrix, which is reduced according to plane strain assumptions and renders the model infinite in the collapsed dimension.

(3) The scattering phenomena, which aren't fully reproduced. For example, Rayleigh scattering is a 3D phenomenon which is closely linked to the scattering cross-section which is proportional to volume and therefore reduced in 2D environments where the scattering can only occur in the two dimensions.

This article presents recent developments of realistically large and detailed FE models of ultrasonic longitudinal wave propagation within polycrystalline materials, demonstrating and evaluating new simulation possibilities in 2D and 3D. It investigates the capability of FE to model the different scattering behaviours across regimes as predicted by the Unified Theory, and assesses the significance of 2D assumptions through comparison with 3D simulations.

This advanced modelling is now becoming possible because of the emergence of sufficiently powerful computing and new, faster modelling tools. Specifically, we make use of a highly efficient GPU based solver[21] for FE which has enabled larger studies e.g. up to 100,000 grains in 2D and 5000 in 3D. Although this approach can be suited to model a variety of microstructures, for this initial investigation, we consider a relatively simple microstructure, untextured, and comprising equiaxed grains of a single phase in a range between 100μm and 500μm. The chosen material is a relatively strong scattering medium, Inconel 600, of cubic symmetry.

As an example of the utility of modelling such as this, recent research[22-24] has raised interesting queries regarding our current understanding of grain scattering, including the role of grains as Rayleigh

scatterers[22] and whether it is not the material imperfections such as voids and inclusions which are contributing to that effect. FE can be useful in this matter by modelling a perfect polycrystalline microstructure, clear of flaws, and identifying the dominant scattering behaviour of the grains.

The subsequent section provides a brief step-by-step outline for FE modelling of polycrystalline materials in 2D, continued by Section 3 which investigates its mesh sampling requirements. Section 4 introduces the 3D model. The main body of results is presented in Section 5 where numerical simulations of a 2D and 3D model are compared to theoretical results obtained from the Unified Theory. Whilst this article does not undertake any experimental investigations, the currently established theory is the culmination of numerous experimental validations e.g.[9,10], in pursuit of grain size characterisation.

II. FE MODELLING OF POLYCRYSTALLINE MATERIAL IN 2-D

Finite Element modelling of polycrystalline materials has been successfully undertaken in various fields of research[25-27] including NDE[16-20] where it has been limited to 2D. Although several approaches have been adopted, all of those mentioned here that consider geometrically varying grains, rely on Voronoi tessellations[28] to numerically generate a morphology which is geometrically similar to a naturally occurring polycrystalline microstructure. This has been accepted as a good approach by researchers in crystallography and textured materials[29]. The next sub-sections provide a brief step-by-step description, and considerations for the aforementioned modelling approach, in 2D.

A. Generating Random Polycrystals

Generating a random polycrystalline microstructure, as achieved in[16-20], starts by randomly distributing points, or seeds, in a 2D Euclidian space. An example of this is shown in Figure 1a where the seed density will determine the resulting average grain size. The coordinates of each seed become the site for a single grain by serving as an input to the Voronoi algorithm[28]. The algorithm subdivides the original space into regions, in the form of convex polygons, whereby each polygon encloses the area which is nearest to that particular seed (see Figure 1b). Once a Voronoi tessellation has been generated, depending on the type of mesh, it requires modification to make it suitable for FE modelling. This procedure involves clipping the boundaries for instance, previously described as regularization[26].

B. 2D considerations

When 3D models are not feasible, reducing a polycrystalline material to a 2D model (see Figure 1c) introduces certain simplifications. This includes the grain size distribution, which impacts, amongst other properties, the ultrasonic characteristics of the material. Whereas for 3D modelling approaches, the simple approach is to match the distribution of grain dimensions to that of the desired material, in 2D, this is not as trivial. Namely, a random cutting plane through a 3D tessellation of grains will not intersect every grain through its centre, rather, some intersections will occur off-centre and therefore reproduce smaller cross-sections. The study of interpreting 2D representations of 3D grains forms the basis of stereology[30] and is beyond the scope of this study. Here, we will assume a normal distribution of grain sizes in 2D (defined as the square root of area), as the one depicted in Figure 2, which assumes that our slice of a 3D material cuts every grain through its centre and therefore overestimates the grain sizes that would be seen in a proper 2D section. Whilst larger grains will increase the attenuation, we are making no claims regarding how this may compare to attenuation of a 3D material. Namely, it would be interesting as a future exercise to further investigate the opportunities and advantages of adjusting grain size distributions in 2D to better match the ultrasonic behaviour of a 3D material; this would be important for rigorous modelling in 2D and is by no means straightforward to achieve.

The orientation distribution function (ODF) of a polycrystalline material is another factor which determines macroscopic properties. For a single phase material, each crystallite should be assigned the same anisotropic stiffness properties but with a random crystallographic orientation to define a macroscopically isotropic material (see Figure 1d). To achieve this, the three reference Euler angles, which define orientation, may be randomly distributed such that their orientations lie equally spaced on the surface of a sphere, as explained by Shahjahan[17] for example. Figure 3 shows the result of rotating orientation angles in 3D for 2000 grains, illustrated by polar plots. As can be seen, as desired, a macroscopically isotropic material has been achieved.

Finally, the 2D simplification leaves two possibilities, one in which the orientation distribution is only in the plane, hence a plane strain model is possible; the other in which the distribution is in 3D, and then needs to be approximated for 2D. Plane strain assumptions then neglect the stiffness constants

associated with the third dimension, when reducing the stiffness matrix from 3D to 2D. The latter is adopted here.

C. Mesh Generation

The minimum FE mesh discretisation for accurate modelling of wave propagation is usually constrained by the wavelength[31]. In this case however, whether using a structured or unstructured mesh, the objects to model, the crystallites, are often an order of magnitude smaller than the wavelength, which demands denser meshes which far exceed the said wavelength criteria. Two possibilities exist, which have previously each been adopted, either an unstructured mesh utilizing triangular FE elements (see Figure 4a) to conform to the complex boundaries of the Voronoi tessellation, or an approximation of the grains with a structured mesh[17] (see Figure 4b). The hazard with a structured mesh is that it leads to "staircasing" effects[31] which become a poor approximation at coarse mesh densities and can lead to tip diffraction from edges, and also to disproportionately strong reflections from waves that are normally incident to the plane of the flats. When using an unstructured mesh however, the challenge is to maintain high quality triangles, i.e. close to equilateral shapes, such that there is minimal mesh scattering. For this purpose, several software solutions are available; for example the authors have found good results, both in terms of the quality of meshes (no large deviations from equilateral, no large variations in element sizes) and the time required to generate them, using a Free software tool, Triangle[32].

D. Efficient Simulations using GPU

Due to the increased mesh density, FE modelling of polycrystalline microstructure is computationally expensive. To reduce this cost and thereby enable parametric studies, the work here employs a relatively new FE solver, Pogo[21]. Pogo exploits the sparsity and highly parallelizable nature of the time explicit FE method, which allows the very efficient use of graphical processing units (GPUs) instead of conventional computer processing units (CPUs) to execute the computations in parallel. It has been shown that this can result in speed improvements of up to two orders of magnitude[21] when compared to commercially established CPU equivalent software. For example, timing of a typical simulation undertaken in this article, when running a 6.1×10^6 degrees of freedom model, was measured to be 67

times faster using 4x Nvidia GTX Titan graphics cards when compared to 2x Intel Xeon 8-core E5-2690 2.9GHz CPUs using general purpose CPU software.

III. MESH VALIDATION FOR 2D

Here we investigate the spatial sampling requirements for both types of mesh mentioned in Section 2.3 to guarantee sufficient modelling accuracy whilst also preserving computational cost. In order to achieve this, both the mesh scattering (Section 3.1) and mesh convergence (Section 3.2) are evaluated for a plane wave model.

The studies in the following Sections 3.1 and 3.2 rely on three different realisations of a polycrystalline material, Inconel 600, using the material properties taken from Shahjahan[17] and shown in Table 1. Each model consists of a different average grain size: 100μm, 250 μm and 500 μm. As computational costs increase for finer grains, this range was limited to keep costs manageable whilst also representing a range of grain sizes of interest to NDE.

Figure 5 shows an example simulation by one of the models used in the study. It is a coarse-grained material represented in 2D by a strip 42mm long and 12mm wide in plane strain. A 3-cycle-toneburst with a 2MHz centre-frequency is applied to the line of nodes, at the left side where x=0mm, which forms the excitation line-source. The model uses symmetry boundary conditions at the top and bottom edges (where y=0mm and y=12mm in Figure 5) such that the nodes are constrained in the y-direction. This creates a plane wave which can be seen to propagate in the positive x-direction. The backscatter can be recognised from the random fluctuations in amplitude trailing the plane wave.

A. Mesh Scattering

Successful simulation of grain scattering can only be achieved if the scattering from element boundaries, here termed mesh scattering, is significantly less than the grain scattering itself. Mesh scattering arises from heterogeneity introduced by irregular element shapes, such as those encountered in unstructured meshes, and can be reduced by increasing mesh density at the cost of additional computation. In order to assess this, we run some unstructured mesh models for which the grain noise

is eliminated, so that the noise is solely due to mesh scattering. This is achieved by assigning isotropic stiffness properties to the grains in this part of the study.

To quantitatively compare results for different mesh densities, the mesh noise is represented by considering the average backscatter energy received by all of the individual nodes. This is calculated from both the temporally and spatially averaged intensity i.e. the root-mean-square (RMS) value of the time-domain backscatter received at the different nodal positions, denoted by S_{rms}. The signal is windowed such that it corresponds to a time after the excitation signal and before the arrival of the reflected signal, which represents a time window where the received energy, in absence of mesh scattering, is anticipated to be zero. For clarity, this is analogous to analysing a time window in-between the frontwall and backwall of a typical pulse-echo time trace encountered in ultrasonic NDE. A worthwhile remark here is that the noise is combined such that it corresponds to the backscatter seen by infinitesimal receivers, whereas in more practical simulations, the mean displacement response across multiple nodes may be considered. Thus this is a relatively harsh case to present, but nevertheless allows useful comparisons.

Figure 6 plots the mean mesh scattering noise (in dB, with reference to the peak of the excitation signal), S_{rms} as a function of the mean element edge divided by the wavelength, $e\lambda^{-1}$, or elements per wavelength. As expected, the mesh scattering decreases as the mesh becomes more refined. In general, the mesh scattering is very low (i.e. all results here are below -40dB) for the range of investigated mesh densities. The unstructured mesh results seem independent of the grain size used once an initial threshold is exceeded.

It is important to acknowledge that these results do not provide an all-encompassing criterion for mesh refinement. The refinement requirement will be model-specific and depend on the severity of the grain noise and on practical compromises on model size. It is crucial however, to suppress it to a controlled degree and this simple approach allows any candidate case to be evaluated.

Structured meshes, which exhibit no variation in element shape, do not require the above considerations and hence clearly outperform unstructured meshes according to this criteria. However, as they do not

conform to the grain boundaries, it is yet unclear whether they can correctly model the scattering behaviour, which is addressed in the next section.

B. Mesh Convergence

It is also important to achieve adequate convergence of the propagating wave pulse. The same models are used as in the previous section, namely with three different grain sizes, except the anisotropic properties of the grains are now introduced (as described in Section 2.2) and thus the wave will be affected by grain scattering. Two metrics are employed to measure convergence, the centre-frequency attenuation, and the group velocity.

As a measure of the propagating wave, the received displacements are now spatially averaged across all the nodes which lie on the right side edge where x=42mm in Figure 5, emulating a pitch-catch plane-wave configuration. The centre-frequency attenuation convergence is calculated as a difference in amplitude between the peak of the received time-domain Hilbert envelope A and that of the converged solution A_c. The converged solution, A_c, is obtained from the highest available density mesh. Similarly, the measured group velocity V_g, which is calculated from the time-of-flight, as measured from the Hilbert envelope peak, is subtracted from the converged solution V_c. To clarify, an error of 0.05 would correspond to a 5% difference in group velocity from that of the converged solution.

Figure 7 and 8 plot, as a function of the mean element edge length e per mean grain size d, the convergence of the centre-frequency attenuation and group velocity respectively, for three different grain sizes, using a structured (S) and unstructured mesh (F). As can be seen, both attenuation and velocity converge as mesh density is increased and velocity converges quickest. At ten elements per linear grain dimension, both metrics are converged to within 1% error for all grain sizes considered which agrees with the findings of Shahjahan[17] for another type of mesh, a rectangular structured mesh.

The progress of convergence reveals that both meshes converge at a similar rate, although the structured mesh seems to converge more monotonically. In the case for an unstructured mesh, the element size distribution can vary by several orders of magnitude within a single model which results in time stepping disadvantages in comparison to structured meshes. This is due to the need to satisfy the critical

time step[33] throughout the model, defined by the smallest element length e_{min} in the model, which may cause oversampling for other elements which are larger, increasing their chance of accumulating numerical noise.

The results for the different grain sizes are somewhat unexpected, namely, the 100μm model seems to converge at a lower mesh density in comparison to the coarser grains. However, this can be explained by a lower grain scattering induced attenuation for the grain size model of 100μm (which has a larger wavelength to grain size ratio), and hence at coarse mesh densities, the mesh scattering, in that specific case, introduces similar levels of attenuation. It can also be noted that convergence for the 500μm grain model initiates with a relatively small error which increases before eventually converging again. Comparing the results for both figures shows however, that at the lowest mesh density, the received signal peak-amplitude may be within 2% of its converged solution (see Figure 7), the group velocity error remains unconverged and at a maximum (see Figure 8). The total attenuation is caused by both mesh and grain scattering (for reference, the mesh scattering induced attenuation will typically be in the order of a few percent for the models simulated here, whereas the grain scattering induced attenuation is typically an order of magnitude larger) , the latter is governed by differences in velocity by adjacent grains. At very low mesh density, the velocity error is large, and the low attenuation we see here may be a fortuitous result due to an artificially increased mesh scattering and reduced grain scattering. In any case, it is clear that we need both velocity and attenuation to be converged for a useful solution.

The authors will refrain from advocating a particular choice of mesh, instead it has been shown that both types are viable options for modelling a polycrystalline microstructure and offer similar performance i.e. offer similar accuracy for the same computational cost. Therefore, the choice for which to use will be largely determined by the particular modelling application, which is also why within the modelling community today, both unstructured and structured meshes are in use. However, for the relatively simple models which will be considered in the subsequent sections, unstructured meshes add unnecessary complications, and hence we have selected structured meshes on this occasion.

IV. FE MODELLING OF POLYCRYSTALS IN 3D

FE modelling of polycrystalline materials in 3D involves the same steps described in section 2, namely a similar Voronoi approach, although the seeds are now distributed in 3D, and a 3D version of the Voronoi algorithm is required. In contrast to 2D modelling, fewer simplifications are necessary to represent the grain property distributions in 3D. However, the computational cost is far greater, and therefore no parametric studies, like those undertaken in the previous section, were feasible. Instead, the knowledge gained from the 2D mesh studies, regarding the mesh requirements, was used to create a 3D model.

The model created here measures 4x4x40mm and counts 5210 randomly orientated Inconel grains with an average grain size of 500µm. For a closer view, only a slice of the full model is shown in Figure 9 which was created using Neper[26]. Similarly to the 2D model, a plane wave is created by imposing symmetric boundary conditions on the rectangular plane surfaces of the model and applying a 3-cycle tone burst to the nodes which lie on the end-surface, seen as a square plane surface at the end of the picture in Figure 10. The key statistics of the model are shown in Table 2. Once the model is solved, post-processing involves calculating the mean nodal displacement of the nodes which lie on the end-face opposite to the excitation plane, thereby emulating a pitch-catch configuration. The results of this procedure and 2D models are discussed in the next section**.**

V. VALIDATION AND COMPARISON OF 2D AND 3D

The numerical results are evaluated for 2D and 3D FE models, adopting structured meshes on this occasion, and comparing their results with expectations from theory. Similarly to the mesh convergence study, both attenuation and velocity are measured, except that now both the attenuation and the phase velocity are evaluated as functions of frequency.

The theoretical values were obtained by computing the complex longitudinal propagation constant as defined by the Unified Theory[9] using the material properties outlined in Table 1. Our implementation was validated by reproducing both results (the attenuation and phase velocity plots) for another cubic polycrystalline material, iron, presented in the original article[8].

The 2D FE models consist of six different models, three for each grain size, 100μm and 500μm, and each excited by a different centre-frequency 3-cycle-toneburst. The range of frequencies applied (see Table 2) are believed to represent a good range of interest, and were limited by increases in computation costs. The single 3D FE model, detailed in Section 4, is solved for various centre frequency excitations in the range of 1-3MHz. Both 2D and 3D model parameters are detailed in Table 2. To enable comparisons to theoretical results which provide results for a mean field, analogous to an infinite plane wave, the dimensions of each FE model are adjusted to ensure sufficient spatial averaging of the received displacements and reduce the effect of phase aberrations and noise. This is a demand which grows with frequency and grain size, thereby increasing computation costs, and therefore defined the frequency range of interest for this article. Similarly, although multiple realisations would ideally be considered to gather more statistics, only one realisation is considered here. Nevertheless, since a large number of grains are considered in each realisation, we do not expect to see significantly large variations in determined quantities, such as the attenuation and phase velocity.

A. Attenuation

We start by comparing the 2D and 3D FE results. The numerical attenuation is calculated by comparing the two frequency spectra corresponding to the transmitted signal and the pitch-catch received signal. This can be achieved by Fast Fourier transforming the windowed time-domain signals and dividing the resultant frequency amplitudes, as explained by Kalashnikov[34] for example. Figure 11 shows attenuation against frequency for three cases. The results show that attenuation increases with both frequency and grain size, which suggests, at least initially, a good qualitative fit with the expected behaviour. By also plotting the power fitting coefficients for each simulation curve, we can further evaluate the results and determine the dominant scattering mechanism. This indicates that a fourth order frequency dependence for the Rayleigh regimes is only produced for the 3D simulation, whereas in 2D, only values close to three are produced. This might be explained by the 2D simplification, where the scattering cross-section is now proportional to the area and not volume of the grain; we expect that this would reduce the Rayleigh scattering to a third order frequency dependence in 2D, according to, for example the observations by Chaffai[36], although we are not aware of formal proof. . This also confirms

that the grains behave as Rayleigh scatterers and shows that, in this specific case, other scatterers, such as voids or material imperfections were not required to explain the dominance of Rayleigh scattering at low frequencies[22].

Now we can compare the attenuation in the simulations to the theoretically predicted equivalent. According to the approach outlined by Stanke[9], the results are normalised such that they are independent of the mean grain size d. In Figure 12, the attenuation coefficient α, normalised through multiplication with d, is plotted against the normalised frequency (product of wavenumber k and d) on a log-log scale. Some ambiguity exists regarding the appropriate choice of d, as previous works[16] have used several values, namely, the mean grain size plus/minus one standard deviation of the grain size to match numerical and theoretical results. Although the choice of d significantly affects the results, in this work we have only used the mean grain size to normalise the results.

The Unified Theory, as shown in Figure 12, indicates the three scattering regimes; Rayleigh for $kd<<1$, stochastic $kd\approx1$, and geometric $kd>>1$, which can each be recognised from their respective gradients, m, relative to their anticipated frequency dependence. In between the Rayleigh and stochastic regime, a transitional regime[9] exists where the frequency dependence can vary before converging to the stochastic asymptote.

As can be seen in Figure 12, the numerical results show good agreement with the established theory suggesting FE has the capacity to model the changing scattering behaviours across frequency. The match is not perfect, however, since the 3D model underestimates and overestimates at low and high frequency respectively. In this case, the 2D model seems to agree slightly better with the theory, but the difference is marginal, and as previously mentioned, largely dependent on the choice of d. This would suggest that even with a simple assumption which overestimates the grain size, good matching with the behaviour of a 3D material is possible. Given the complex and random nature of these materials, these results are considered to be satisfactory.

B. Phase Velocity

Along with a complex frequency-dependent attenuation, propagating elastic waves in these materials exhibit small changes in phase velocity. Here we compare predictions of the Unified Theory to numerical results for phase velocity, obtained by comparing the phase angles of the transmitted and received signal. This can be achieved by Fast Fourier transforming the windowed time-domain signal and subtracting their unwrapped phase as explained by Kalashnikov[34] for example.

Figure 13 shows phase velocity as a deviation from the Voigt velocity[35], which is an average velocity for an equivalent macroscopically isotropic medium, calculated from the material elastic constants in Table 1. The x-axis plots the same logarithm of normalised frequency log*(kd)* as described in the previous section.

The results show that FE matches well with the Unified Theory, and there is good trend matching in the dispersive region, which is accurate to within 1%. The 3D results suggest a better match than 2D in this case.

VI. CONCLUSIONS

This article has set out to present and asses new progress in capabilities of Finite Element (FE) modelling to simulate ultrasonic scattering of longitudinal waves in an equiaxed and untextured polycrystalline material, for both 2D and 3D. The modelling adopts an established Voronoi approach to randomly generate a representative grain layout. Relying on a recently developed GPU FE solver, Pogo, large parametric studies in 2D and a single 3D model became feasible. The 2D parametric studies illustrated the mesh sampling requirements for two different types of mesh and different levels of mesh refinement, to ensure modelling accuracy and present useful guidelines for future modelling of these materials. During comparison to established theory, for both 2D and 3D, the numerically calculated attenuation and phase velocity showed good agreement across a range of scattering regimes. This suggests that even with relatively simple descriptions of these materials, this type of numerical modelling has the ability to capture the key physics. Modelling limitations were also found. It was shown that 2D models reduce the scattering mechanism in the Rayleigh regime. Overall, it is proposed

that the progress and understanding presented in this article will aid the ongoing improvement of FE simulations of ultrasonic NDE of polycrystalline materials.

VII. ACKNOWLEDGEMENTS

The authors are grateful to Professor Peter Nagy from the University of Cincinnati and Dr. Bo Lan from Imperial College London for the helpful discussions. This work has been supported by the UK Research Centre in NDE, the Engineering and Physical Sciences Research Council grant EP/I017704/1, and E.ON Technologies (Ratcliffe) Ltd.

REFERENCES

1. W.P. Mason, H. J. McSkimin, "Attenuation and scattering of high frequency sound waves in metals and glasses", J. Acoust. Soc. Am. **19**(3), 464-473 (1947).
2. H. B. Huntington, "On ultrasonic scattering by polycrystals", J. Acoust. Soc. Am. **22**, 362-364 (1950).
3. W. Roth, "Scattering of ultrasonic radiation in polycrystalline metals", J. Appl. Phys. **19,** 901-910 (1948).
4. E. M. Lifshits, G. D. Parkhamvoski, "On the theory of ultrasonic wave propagation in polycrystals" (in Russian), Zh. Eksp. Teor. Fiz. **20**, 175-182 (1950).
5. A. B. Bhatia, R. A. Moore, "Scattering of High Frequency Sound Waves in Polycrystalline Materials II", J. Acoust. Soc. Am. **32**(1), 1140-1141 (1959).
6. L. L. Rokhlin, "Scattering of Ultrasound in Polycrystalline Materials", Soviet Physics – Acoustics **18**(1), 71-75 (1972).
7. S. Hirsekorn, "The scattering of ultrasonic waves by Polycrystals", J. Acoust. Soc. Am. **72**(3), 1021-1031 (1982).
8. F. E. Stanke, G. S. Kino, "A unified theory for elastic wave propagation in polycrystalline materials", J. Acoust. Soc. Am **75**(3), 665-681 (1984).
9. F. E. Stanke, "Inversion of attenuation measurements in terms of parameterized autocorrelation function" in *NDE for Microstructure Process Control*, ed. by H. N. G. Wadley, (American Society for Metals, Ohio, 1985) p.55.
10. E. P. Papadakis, "Ultrasonic attenuation caused by scattering in polycrystalline media" in W.P Mason (Ed.), *Physical Acoustics vol 4 part B* (Academic Press, NY, London, 1968) 269-328.

11. R. B. Thompson, F. J. Margetan, P. Haldipur, L. Yu, A. Li, P. Panetta, H. Wasan, “Scattering of elastic waves in simple and complex polycrystals”, Wave Motion **45**(5) 655-674 (2008).
12. J. H. Rose, "Ultrasonic backscatter from microstructure" in *Review of Progress in Quantitative Non-destructive Evaluation*, Vol. 11, D. O. Thompson and D. E. Chimenti, Eds (Plenum Press, NY, 1991), pp. 1677-1684 .
13. F. J. Margetan, R. B. Thompson, I. Yalda-Mooshabad, “Backscattered microstructural noise in ultrasonic toneburst inspections”, J. Nondestruct. Eval. **13**(3), 111-136 (1994).
14. F. J. Margetan, J. Umback, R. Robert, A. D. Friedl, M. Keller, W. Hassan, L. Brasche, A. Klassen, H. Wasan, A. Kinney, 2007, “Inspection Development for Titanium Forgings – Engine Titanium Consortium”, FAA William J. Hughes Technical Center, Atlantic City, N. J. Report DOT/FAA/AR-05/46 (2007).
15. L. Anxiang, R. Roberts, P. Haldipur, F. J. Margetan, R. B. Thompson. "Computational study of grain scattering effects in ultrasonic measurements" in *Review of Progress in Quantitative Nondestructive Evaluation,* ed. by D. O. Thompson and D. E Chimenti, American Institute of Physics Conference Proceedings **657**, 117-127 (2003).
16. G. Ghoshal, J. A. Turner, “Numerical model of longitudinal wave scattering in polycrystals”, IEEE Trans. Ultrason., Ferroelectr. Freq. Control **56**(7), 1419-1428 (2009).
17. S. Shahjahan, F. Rupin, A. Aubry, B. Chassignole, T. Fouquet, A. Derode, “Comparison between experimental and 2-D numerical studies of multiple scattering in Inconel600® by means of array probes” Ultrasonics **54**(1), 358-367 (2014).
18. B. Chassignole,V. Duwig, M.-A. Ploix, P. Guy P., R. El Geurjouma, “Modelling the attenuation in the ATHENA finite elements code for the ultrasonic testing of austenitic stainless steel welds”, Ultrasonics **49**(8), 653-658 (2009).

19. B. Lan, M. Lowe, F. P. E Dunne, “Experimental and computational studies of ultrasound wave propagation in hexagonal close-packed polycrystals for texture detection” Acta Materialia **63**(15)**,** 107-122 (2014).
20. N. Feuilly, O. Dupond, B. Chassignole, J. Moysan, and G. Comeloup. "Relation between ultrasonic backscattering and microstructure for polycrystalline materials" in *Review of Progress in Quantitative Nondestructive Evaluation,* ed. by D. O. Thompson and D. E Chimenti, American Institute of Physics Conference Proceedings **1096**, 1216-1223 (2009).
21. P. Huthwaite, “Accelerated finite element elastodynamic simulations using the GPU”, Journal of Computational Physics **257**, 687-707 (2014).
22. X.-G. Zhang, Simpson W. A., Jr. and J. M. Vitek, Barndard D. J., Tweed L. J., Foley J., “Ultrasonic attenuation due to grain boundary scattering in copper and copper-aluminium” J. Acoust. Soc. Am. **116**(1), 109-116 (2004).
23. F. Zeng, Agnew S.R., Raeisinia B., Myneni G.R., “Ultrasonic attenuation due to grain scattering in pure niobium”, J. Nondestruct. Eval. **29**(2), 93–103 (2010).
24. M. Agnès, V. Pagneux, D. Boyer, F. Lund, "Propagation of elastic waves through polycrystals: the effects of scattering from dislocation arrays", Proc. R. Soc. A **462** no. 2073, 2607-2623 (2006).
25. P. Zhang, D. Balint, “An integrated scheme for crystal plasticity analysis: Virtual grain structure generation”, Computational Materials Science **50**(10), 2854-2864 (2011).
26. R. Quey, P. R. Dawson, F. Barbe, “Large-scale 3D random polycrystals for the finite element method: Generation, meshing and remeshing”, Computer Methods in Applied Mechanics and Engineering **200**, 1729-1745 (2011).
27. M. Kamaya, “A Procedure for estimating Young’s modulus of textured polycrystalline materials” International Journal of Solids and Structures **46**(13), 2642-2649 (2009).

28. F. Aurenhammer, “Voronoi diagrams—a survey of a fundamental geometric data structure”, ACM Computing Surveys (CSUR) **23**(3), 345-405 (1991).
29. F. U. Kocks, C. N. Tomé, H-R. Wenk, *Texture and anisotropy: preferred orientations in polycrystals and their effect on materials properties* (Cambridge University Press, Cambridge, 2000) p. 668.
30. E. E. Underwood, *Quantitative Stereology* (Addison-Wesley, Reading, 1970) p.274.
31. M. Drozdz, *Efficient finite element modelling of ultrasound waves in elastic media*, (Ph.D. dissertation, Imperial College of Science and Technology and Medicine, 2008).
32. J. R. Shewchuk, “Delaunay Refinement Algorithms for Triangular Mesh Generation”, Computational Geometry: Theory and Applications **22**(1-3), 21-74 (2002).
33. K. J. Bathe, *Finite Element Procedures* (Prentice Hall, New Jersey, 1996) p. 1037.
34. A. Kalashnikov, R. E. Challis, “Errors and uncertainties in the measurements of ultrasonic wave attenuation and phase velocity” IEEE Trans. Ultrason., Ferroelectr. Freq. Control **52**(10), 1754-1768 (2005).
35. W. Voigt, *Lehrbuch der Krystallphyskik* (Textbook on Crystallography) (Teubner, Leipzig, 1928) p. 962
36. S. Chaffai, V. Roberjot, F. Peyrin, G. Berger, P. Laugier, “Frequency dependence of ultrasonic backscattering in cancellous bone: Autocorrelation model and experimental results” J. Acoust. Soc. Am. **108**(5), 2403- 2411 (2000).

Material Property	Inconel 600
C_{11}	234.6 GPa
C_{12}	145.4 GPa
C_{44}	126.2 GPa
ρ	8260 kg/m^3

Table 1: Material constants for cubic Inconel 600[17].

Model	2D D=100μm			2D D=500μm			3D D=500μm
Centre Frequencies	2MHz	3MHz	5MHz	1MHz	2MHz	3MHz	1,2,and 3MHz
Number of grains	60 $x10^3$	100 $x10^3$	100 $x10^3$	30 $x10^3$	23 $x10^3$	25 $x10^3$	5 $x10^3$
Length (mm)	100	50	50	150	75	25	40
Width (mm)	6	20	20	50	75	250	4x4
Degrees of Freedom	12 $x10^6$	20 $x10^6$	31 $x10^6$	5 $x10^6$	8 $x10^6$	8 $x10^6$	$16x10^6$

Table 2: Parameters for three models with different grain sizes, 100 μm and 500μm for two 2D models, and 500 μm for a 3D model.

LIST OF FIGURES

different grain size models, 100μm (triangular maker), 250μm (rectangular marker), 500μm (circular marker). The centre-frequency attenuation can be seen to converge within 1% at approximately 10 elements per grain.

Figure 8: (color online) Normalised group velocity convergence against the number of elements per grain for structured (S) and unstructured meshes (F). Results are shown for three different grain sizes, 100μm (triangular marker), 250μm (rectangular marker), 500μm (circular marker). Both meshes can be seen to converge to within 1% at approximately 6 elements per grain dimension

Figure 9: (color online) Slice (4mmx4mmx10mm) of the 3D model of a polycrystalline material with 500μm average grain size where the shades denote different grains. The full model contains 5210 grains and $16x10^6$ degrees of freedom.

Figure 10: (color online) 3D FE simulation for a plane wave propagating throughout a polycrystalline material, Inconel, with an average 500μm grain size, shown at three different times: 1.5 μs, 3.5μs, and 5μs.

Figure 11: (color online) Frequency dependent attenuation in dB/cm against frequency, for (a) 100μm (b) 500μm grain sized material in 2D and (c) in 3D for 500μm. As expected the attenuation increases with frequency and grain size. The best-fit power coefficient is plotted for all nine (three per model) simulations, where the subscript denotes their centre-frequency in MHz. In the long wavelength to grain size ratios, the power coefficient approaches the Rayleigh result, whilst at higher frequencies, they converge towards the stochastic limit.

Figure 12: (color online) Normalised attenuation coefficient versus normalised frequency for a longitudinal wave in polycrystalline Inconel for for three different models, a 100um 2D (triangular maker), 500um 2D (rectangular maker), and 500um 3D (circular marker). The three different scattering regimes are indicated (dashed lines) with their respective gradients

m. The attenuation results can be seen to compare well to the Unified Theory[8] (black solid line). The empty markers are for labelling purposes only, and hence are not indicative of sampling.

Figure 13: (color online) Normalised variation of longitudinal phase velocity against normalised frequency, for three different models of polycrystalline Inconel, a 100um 2D (traignular marker), 500um 2D (rectangular marker), and 500um 3D (circular marker). The results can be seen to compare well to the Unified Theory[8] for both 2D and 3D finite element results. The empty markers are for labelling purposes only, and hence are not indicative of sampling.

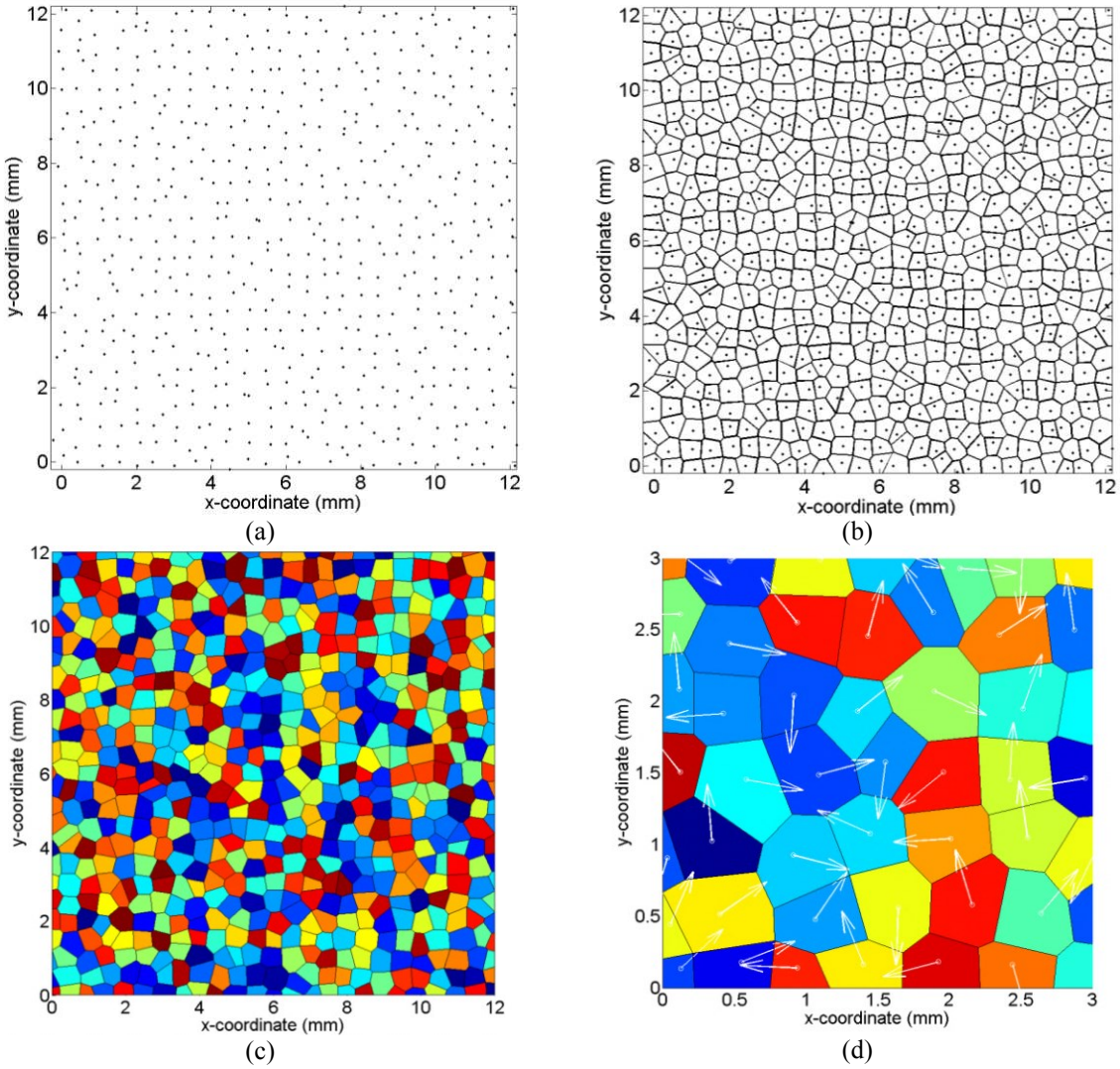

Figure 1: (color online) Illustration of the steps involving a Voronoi generation of polycrystals: (a) a random distribution of seeds; (b) the Voronoi tessellations produced by (a); (c) The regularized grain layout and (d) the random orientations assigned to each grain, here shown by arrows in the 2D plane for clarity (note zoomed scale of this image compared to the others). Colors are only illustrative.

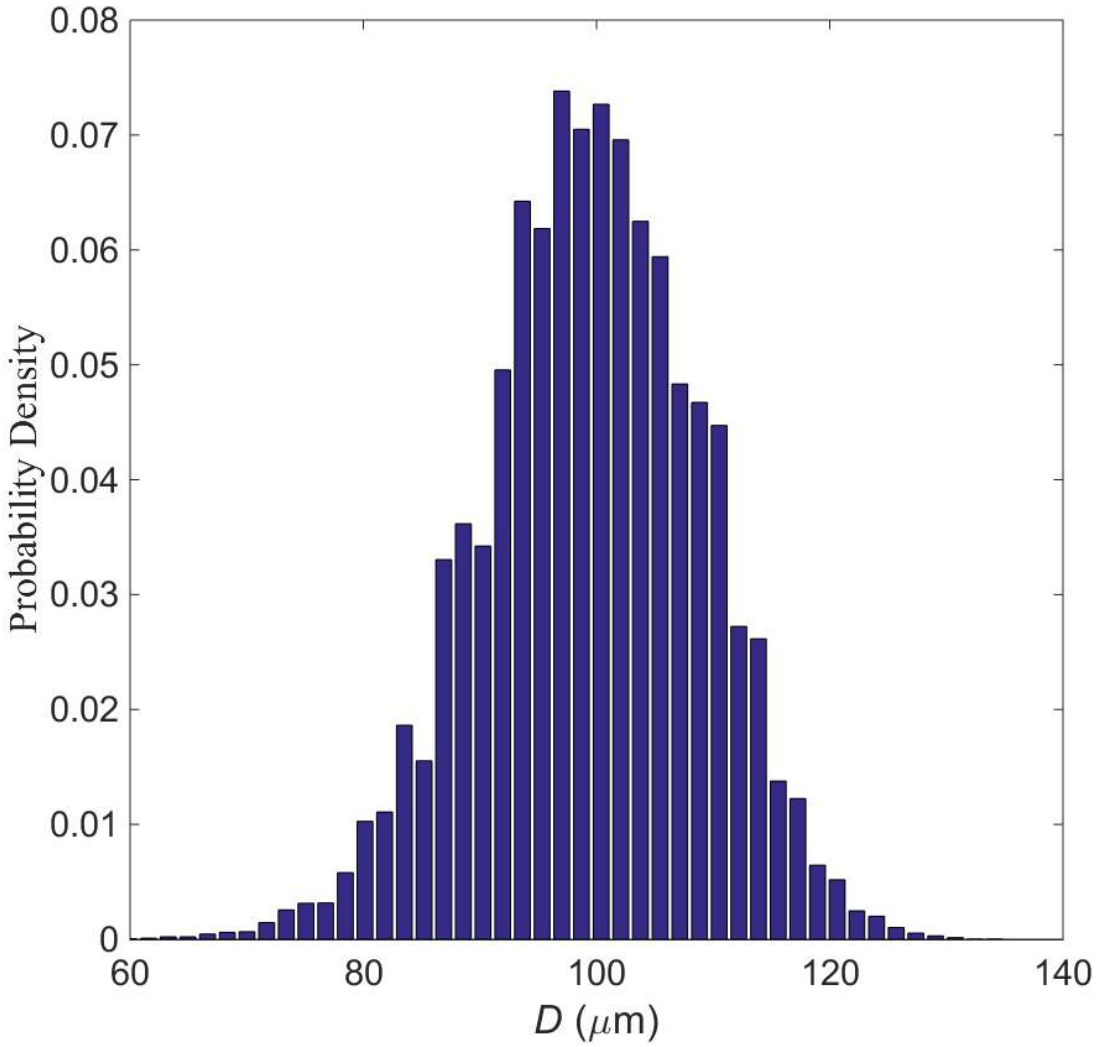

Figure 2: Grain size distribution for a typical random realistation of an input 100μm grain size material. The grain size *D* in this 2D case is defined by the square root of area.

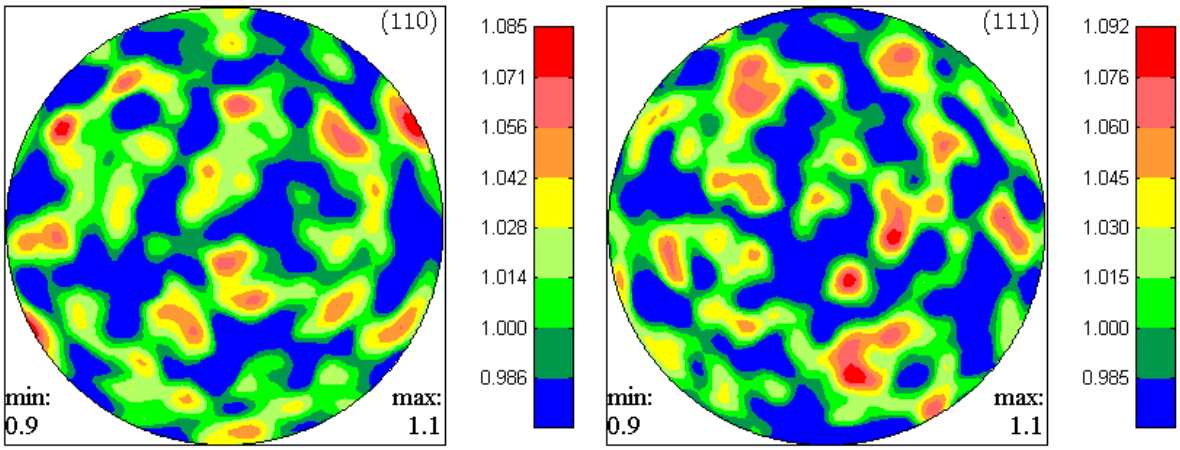

Figure 3: (color online) Typical pole plot (ODFs) for a randomly generated material. The distribution of grain alignments over the whole sphere shows for this example that the generated material is indeed isotropic. The scales indicate the distribution of probability density for the orientation angles of the <110> and <111> crystallographic axis.

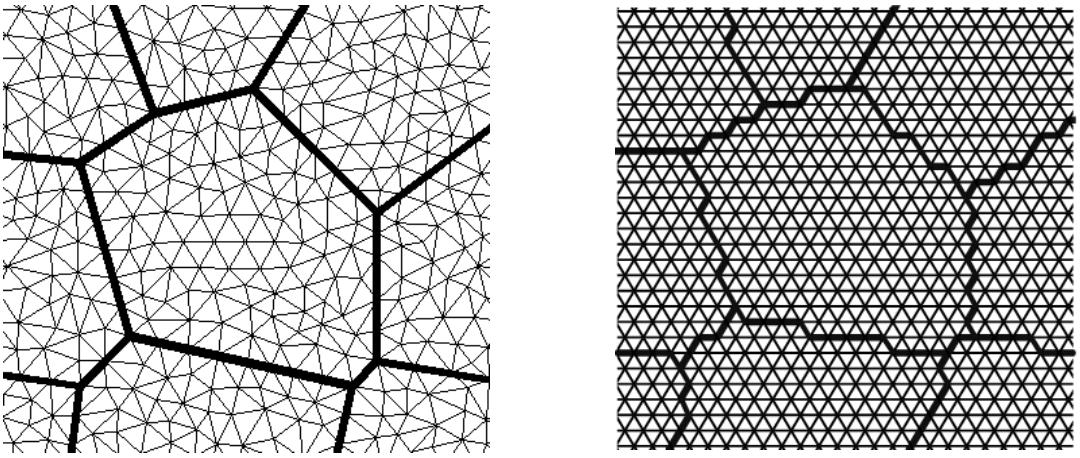

(a) **(b)**

Figure 4: Typical grain meshed using (a) unstructured and (b) structured mesh.

(a)

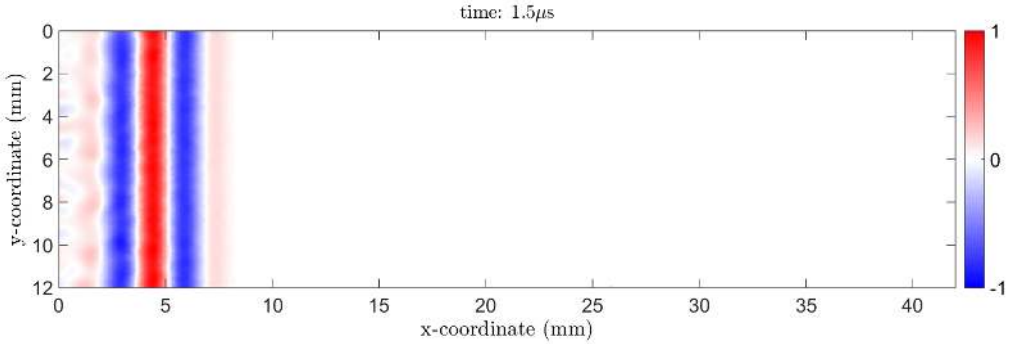

(b)

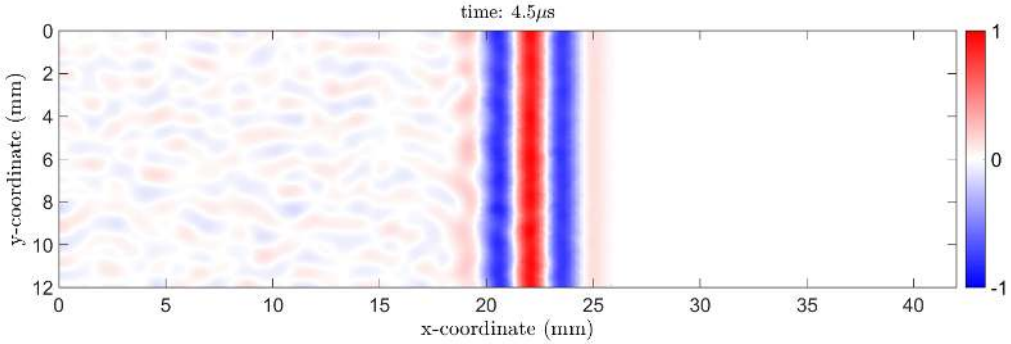

(c)

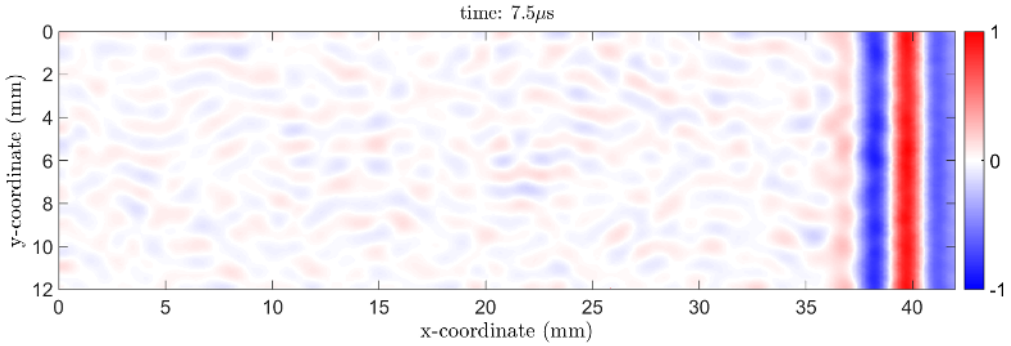

Figure 5: (color online) FE simulation of longitudinal plane wave propagating from left to right within a 2D slab of polycrystalline Inconel for different times after (a) 1.5μs (b) 4.5μs and (c) 7.5μs. The colour scale is the normalised displacement amplitude with reference to the peak excitation amplitude from -100% to 100%.

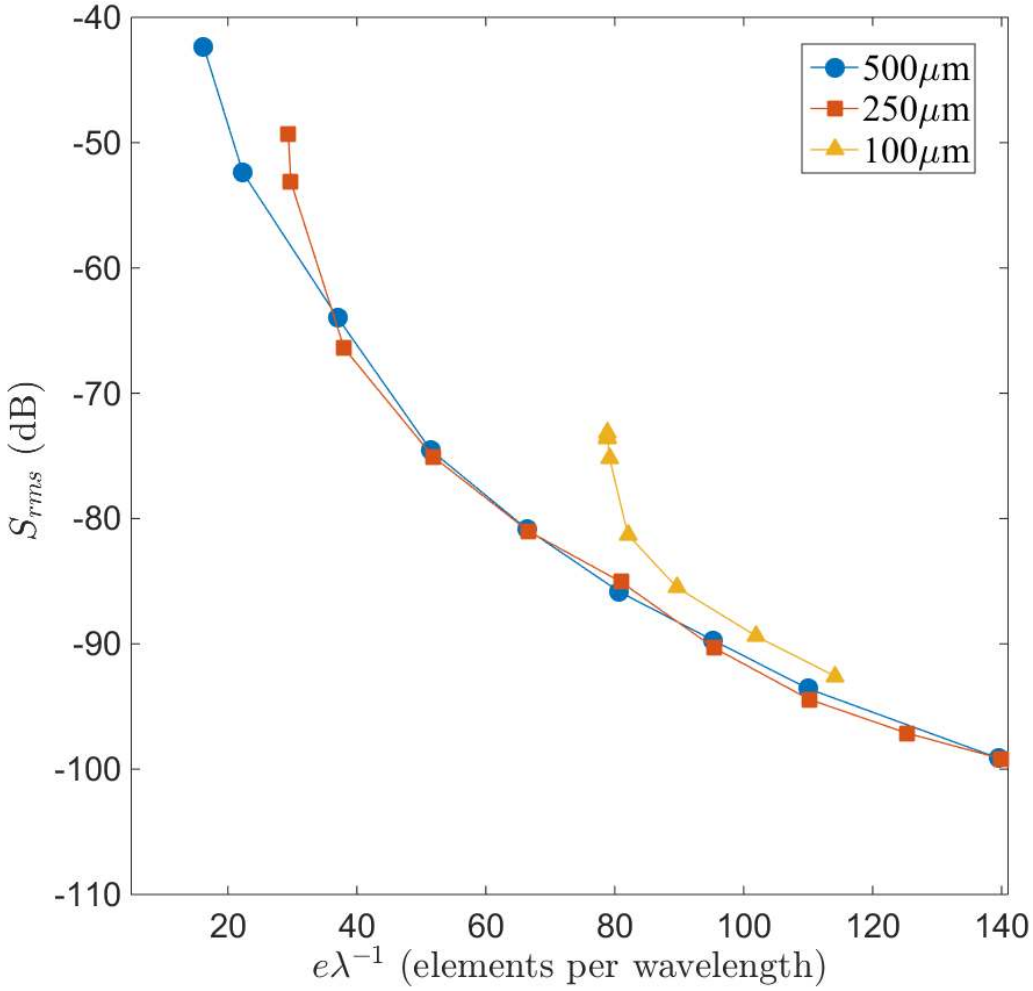

Figure 6: (color online) Mean normalised mesh scattering noise (in dB, with reference to the peak of the excitation signal) versus number of elements per wavelength for several unstructured meshes, each conforming to polycrystalline material with a different average grain sizes.

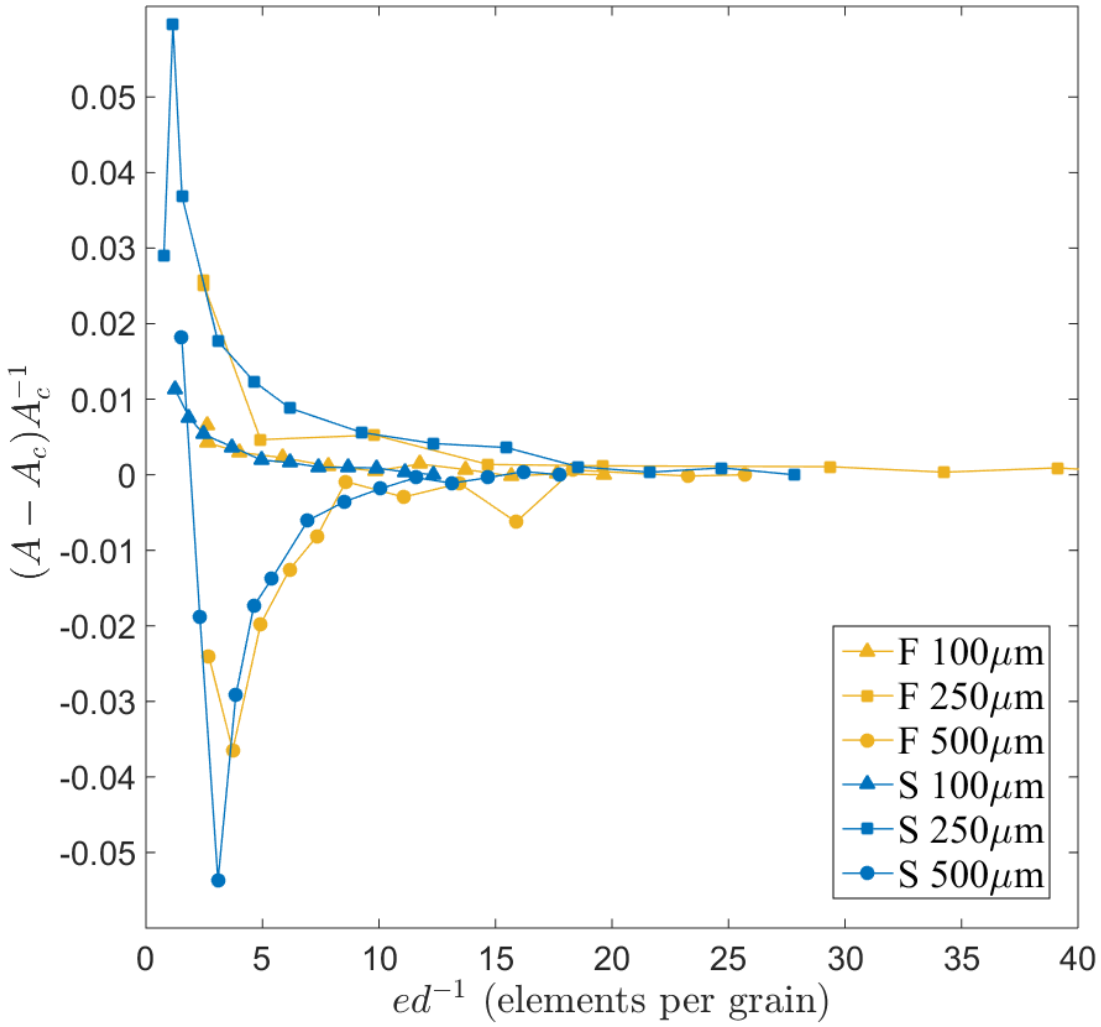

Figure 7: (color online) Convergence of normalised centre-frequency attenuation against elements per grain for structured (S) and unstructured meshes (F). Results are shown for three different grain size models, 100µm (triangular maker), 250µm (rectangular marker), 500µm (circular marker). The centre-frequency attenuation can be seen to converge within 1% at approximately 10 elements per grain.

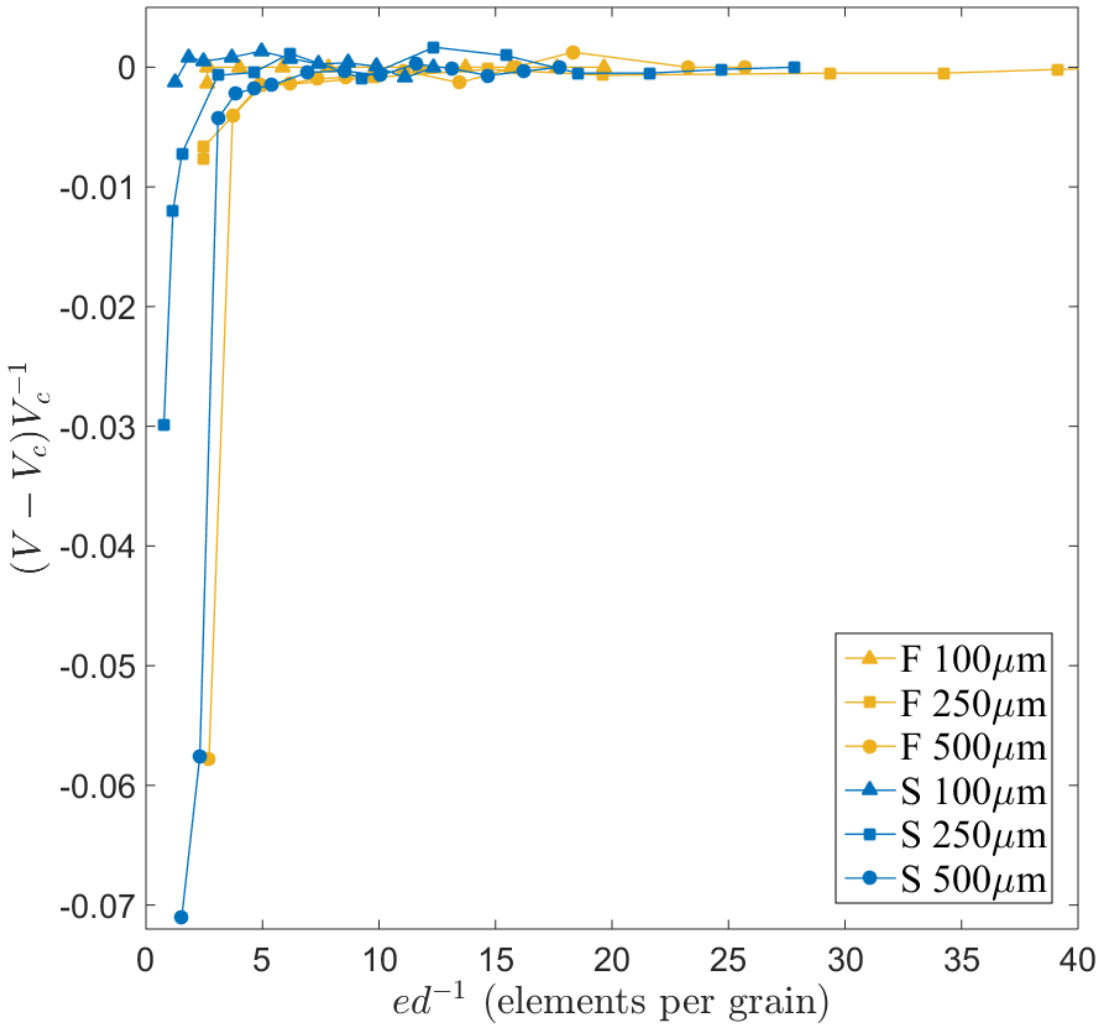

Figure 8: (color online) Normalised group velocity convergence against the number of elements per grain for structured (S) and unstructured meshes (F). Results are shown for three different grain sizes, 100µm (triangular marker), 250µm (rectangular marker), 500µm (circular marker). Both meshes can be seen to converge to within 1% at approximately 6 elements per grain dimension.

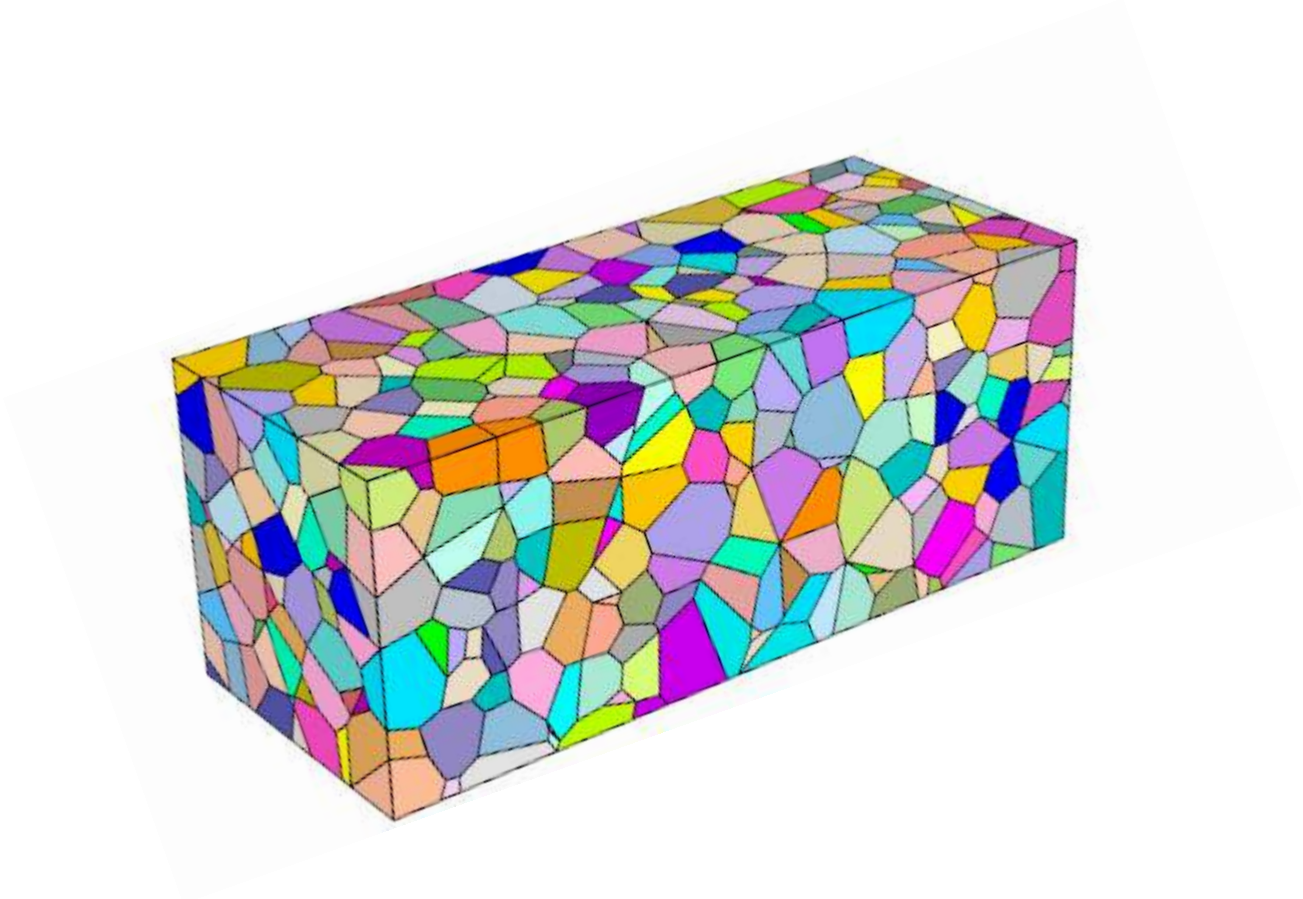

Figure 9: (color online) Slice (4mmx4mmx10mm) of the 3D model of a polycrystalline material with 500μm average grain size where the shades denote different grains. The full model contains 5210 grains and 16×10^6 degrees of freedom.

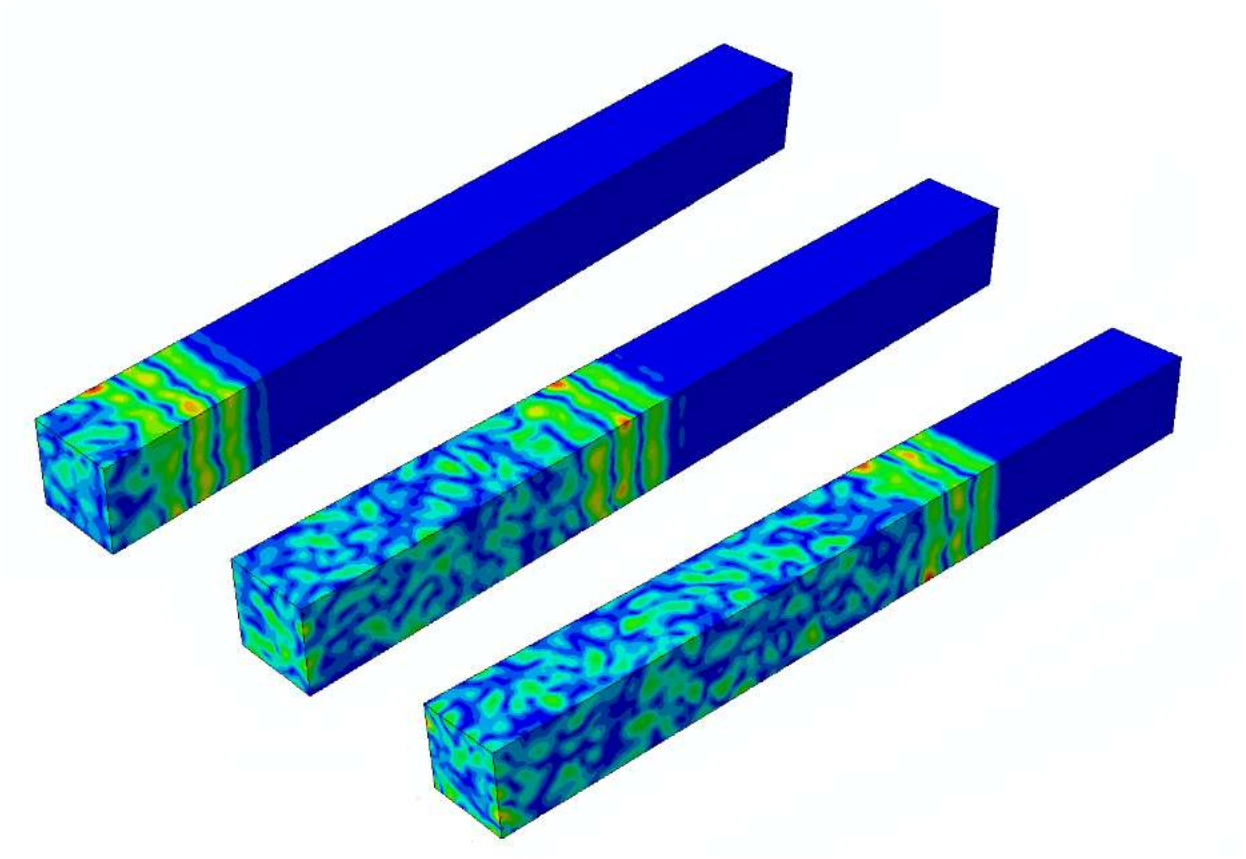

Figure 10: (color online) 3D FE simulation for a plane wave propagating throughout a polycrystalline material, Inconel, with an average 500μm grain size, shown at three different times: 1.5 μs, 3.5μs, and 5μs.

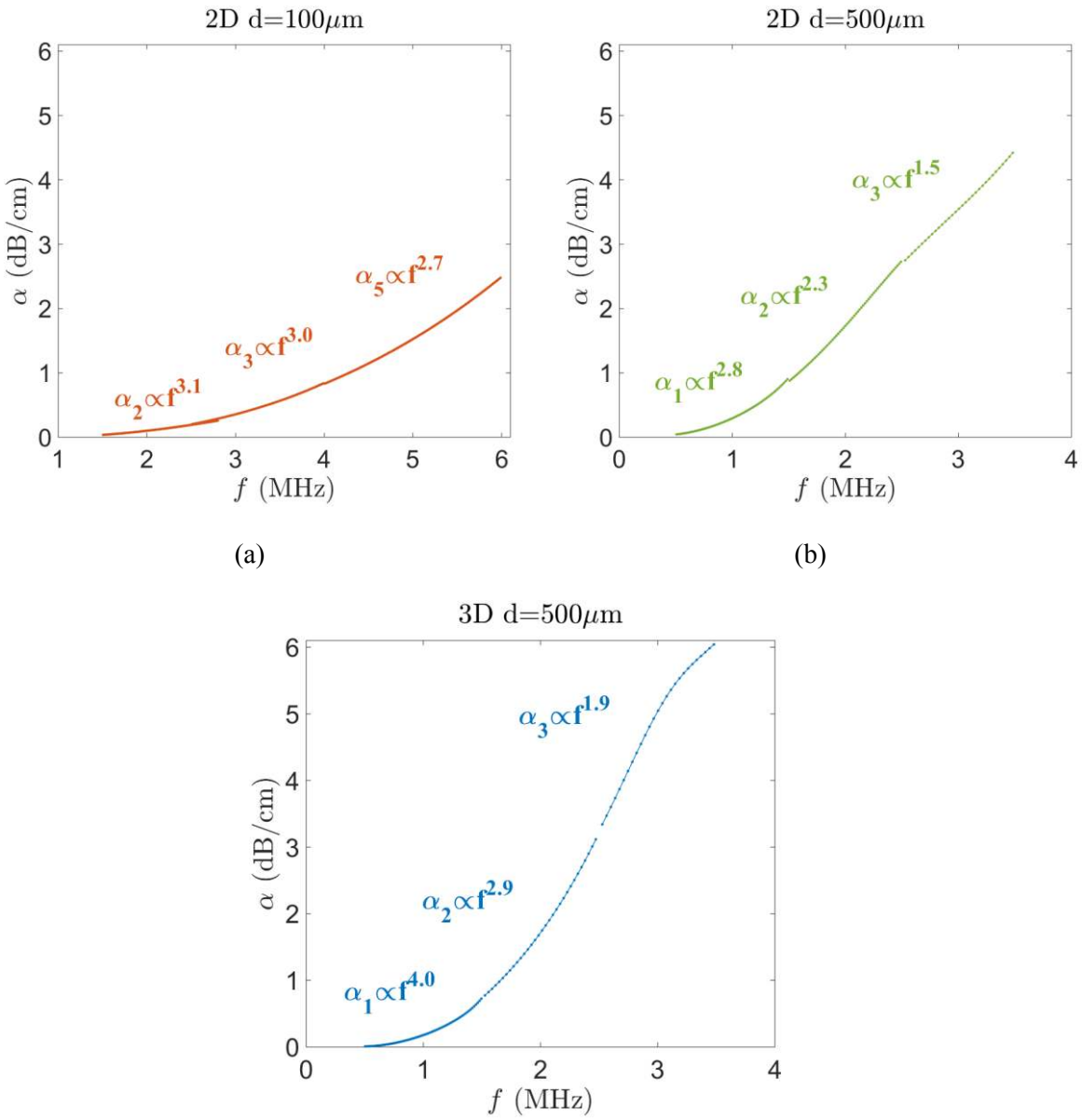

Figure 11: (color online) Frequency dependent attenuation in dB/cm against frequency, for (a) 100µm (b) 500µm grain sized material in 2D and (c) in 3D for 500µm. As expected the attenuation increases with frequency and grain size. The best-fit power coefficient is plotted for all nine (three per model) simulations, where the subscript denotes their centre-frequency in MHz. In the long wavelength to grain size ratios, the power coefficient approaches the Rayleigh result, whilst at higher frequencies, they converge towards the stochastic limit.

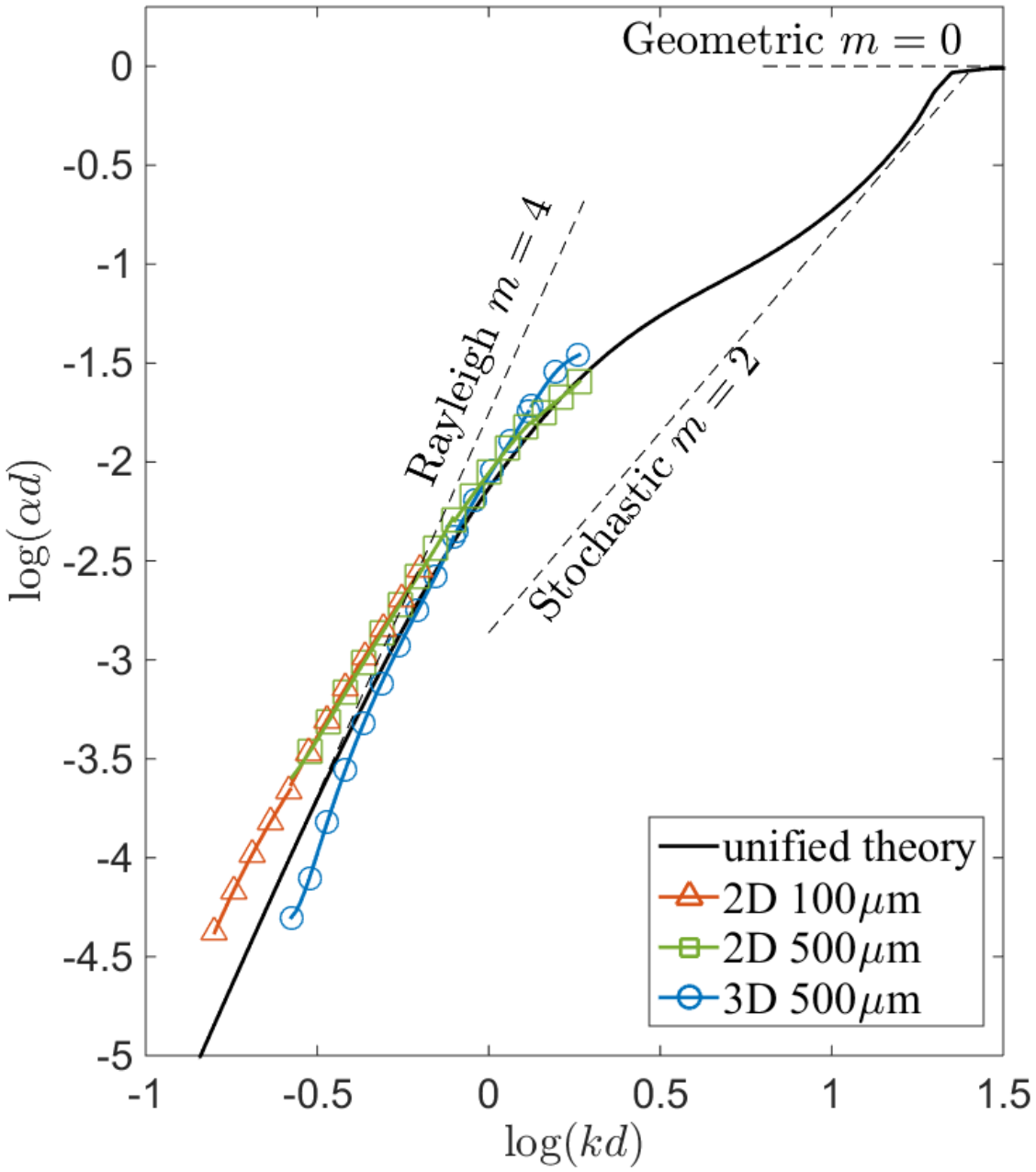

Figure 12: (color online) Normalised attenuation coefficient versus normalised frequency for a longitudinal wave in polycrystalline Inconel for for three different models, a 100um 2D (triangular maker), 500um 2D (rectangular maker), and 500um 3D (circular marker). The three different scattering regimes are indicated (dashed lines) with their respective gradients *m*. The attenuation results can be seen to compare well to the Unified Theory[8] (black solid line). The empty markers are for labelling purposes only, and hence are not indicative of sampling.

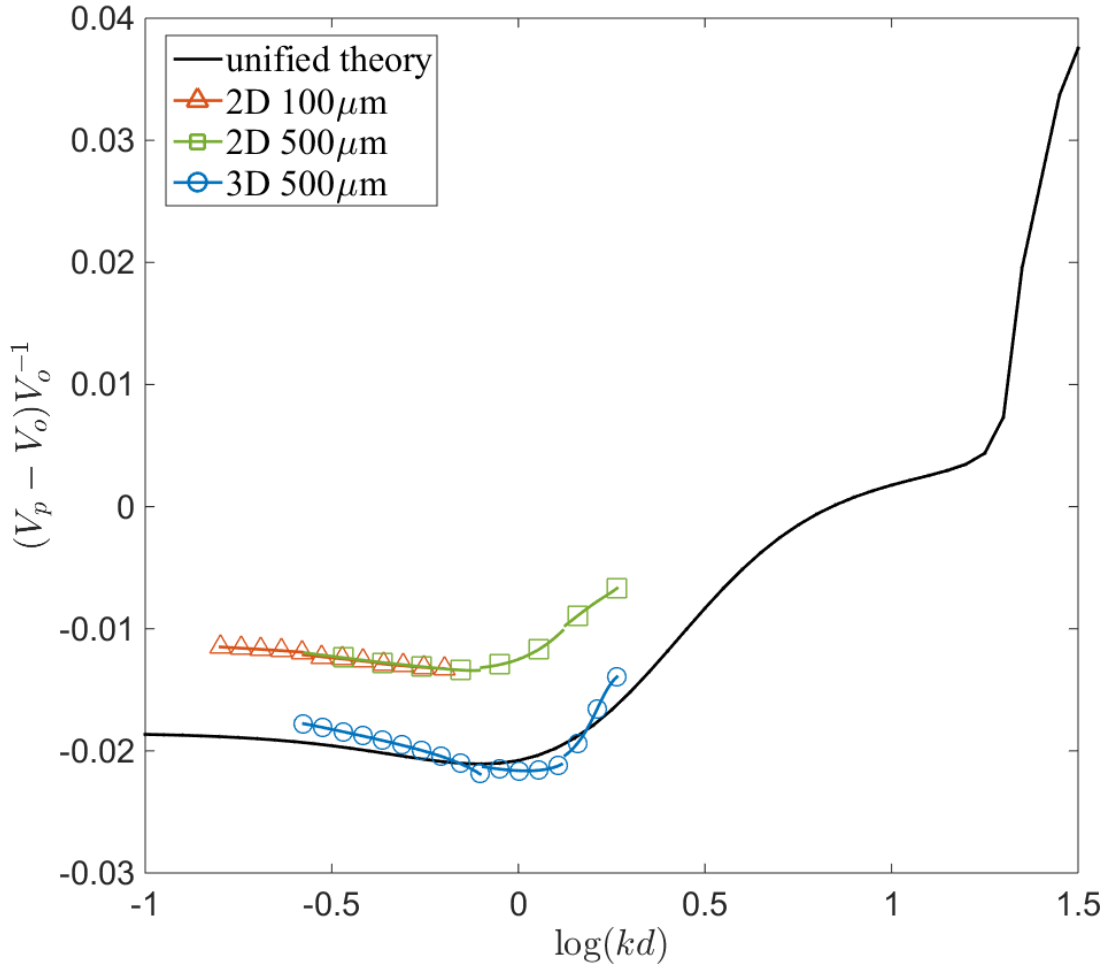

Figure 13: (color online) Normalised variation of longitudinal phase velocity against normalised frequency, for three different models of polycrystalline Inconel, a 100um 2D (triangular marker), 500um 2D (rectangular marker), and 500um 3D (circular marker). The results can be seen to compare well to the Unified Theory[8] for both 2D and 3D finite element results. The empty markers are for labelling purposes only, and hence are not indicative of sampling.